Analysis of quasi-ballistic hole transport capability of Ge and Si nanowire pMOSFETs by a quantum-corrected Boltzmann transport equation

Hajime Tanaka, Jun Suda, and Tsunenobu Kimoto
Department of Electronic Science and Engineering
Kyoto University
Kyoto, Japan
tanaka@semicon.kuee.kyoto-u.ac.jp

***Abstract*—The quasi-ballistic hole transport capabilities of Ge and Si nanowire pMOSFETs were analyzed based on a quantum-corrected Boltzmann transport equation. A new formalism of quantum-correction potential was proposed, and using this model, the current drive capabilities of Ge and Si nanowire pMOSFETs were compared. Though the ON-current was larger in the Ge nanowire pMOSFET, the transmission coefficients are similar between Ge and Si, because the higher hole mobility of Ge is canceled by its slower energy relaxation. Thus, the larger current of the Ge nanowire pMOSFET was attributed to its larger injection current. The impact of device geometry on the performance was also investigated, and the [110]-oriented Ge nanowire pMOSFET with a 15 nm gate length exhibited the highest performance among the devices considered in this study.**

Keywords—quasi-ballistic hole transport; nanowire MOSFET; germanium; silicon; quantum-corrected Boltzmann transport equation

I. Introduction

Ge nanowire (NW) MOSFETs are a promising candidate for future CMOS devices [1] owing to the high mobility of Ge and high electrostatic controllability of NW structure. Thus the carrier transport in Ge NW MOSFETs, especially in the quasi-ballistic regime, is important. In this study, we analyzed the quasi-ballistic hole transport in Ge NW pMOSFETs by a quantum-corrected Boltzmann transport equation (QC-BTE) considering phonon scattering, and the hole transport capability was compared with a Si counterpart. In addition, the impacts of transport orientations and gate length on device performance are investigated.

II. Calculation Method

A. Quantum-Corrected Boltzmann Transport Equation

QC-BTE takes account of quantum effects as a quantum-correction potential V_{Q}. Using V_{Q}, the QC-BTE is given as [2]

$$\frac{\partial}{\partial t}f = \frac{1}{\hbar}\frac{d}{dx}\left[V(x)+V_{\mathrm{Q}}(x)\right]\frac{\partial}{\partial k}f - v_{\mathrm{g}}(k)\frac{\partial}{\partial x}f + \left(\frac{\partial f}{\partial t}\right)_{\mathrm{scat.}} . \quad (1)$$

The formula for V_{Q} proposed in this study is given as follows.

$$V_{\mathrm{Q}}(x) = a(x)\left[\frac{d^2}{dx^2}V(x)\right] + \frac{b(x)}{a(x)}\left[\frac{d^2}{dx^2}V_{\mathrm{Q}}(x)\right] \quad (2)$$

Here, $a(x) \equiv \frac{1}{24}\frac{2}{k_{\mathrm{B}}T_{\mathrm{e}}(x)}\left\langle\frac{d^2E}{dk^2}\right\rangle$, $b(x) \equiv \frac{1}{240}\frac{1}{\left(k_{\mathrm{B}}T_{\mathrm{e}}(x)\right)^2}\left\langle\left(\frac{d^2E}{dk^2}\right)^2\right\rangle$ ($\langle\ldots\rangle$ means averaging by the distribution function f), and $T_{\mathrm{e}}(x) \equiv \frac{\int\left(\frac{dE}{dk}\right)^2 f dk}{\int\frac{d^2E}{dk^2}f dk}$. $V(x) = -e\phi(x)$ is the classical electrostatic potential. Equation (2) was derived from the first ($\alpha = 1$) and second ($\alpha = 2$) quantum-correction terms in the Wigner transport equation [3] in the derivative representation,

$$\frac{\partial}{\partial t}f = \frac{1}{\hbar}\frac{dV}{dr}\frac{\partial}{\partial k}f - v_{\mathrm{g}}(k)\frac{\partial}{\partial x}f + \left(\frac{\partial f}{\partial t}\right)_{\mathrm{scat.}} + \sum_{\alpha=1}^{\infty}\frac{(-1)^{\alpha}}{\hbar 4^{\alpha}(2\alpha+1)!}\frac{d^{2\alpha+1}V}{dx^{2\alpha+1}}\frac{\partial^{2\alpha+1}}{dk^{2\alpha+1}}f. \quad (3)$$

During the formula deformation, assumption of $f \propto \exp(-E/k_{\mathrm{B}}T_{\mathrm{e}})$ was used.

B. Transport Calculation

The valence band structure in NWs was calculated by an $sp^3d^5s^*$ tight-binding approximation [4]. The phonon states were computed by a valence force field model [5], and the electron-phonon interaction was treated atomistically [6]. Considering the scattering rates of phonon scattering calculated by Fermi's golden rule, the time evolution of the hole

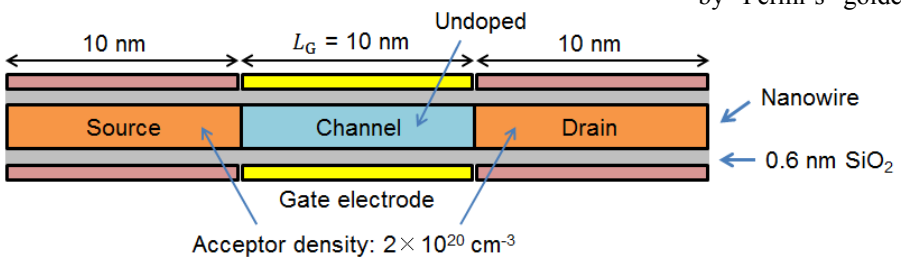

Fig. 1: Schematic image of the device structure of the NW MOSFETs assumed in this study. The source and drain regions are 10-nm-long and doped to 2×10^{20} cm^{-3}, while the channel region is undoped and has L_G = 10 nm unless otherwise stated.

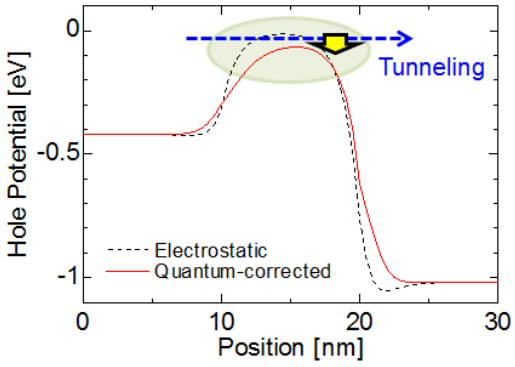

Fig. 2: Calculated electrostatic and quantum-corrected potentials in the Ge [110] NW pMOSFET at the OFF-state. The reduction of potential barrier height due to quantum correction expresses the impact of tunneling.

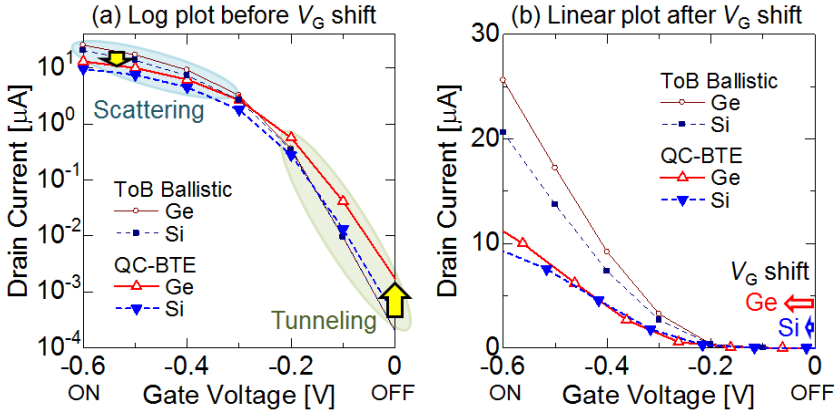

Fig. 3: Calculated gate voltage dependence of drain current in the Ge and Si [110] NW pMOSFETs (a) before and (b) after V_G shift. The results calculated by the quantum-corrected Boltzmann transport equation (QC-BTE) are compared with the ballistic current by the top of the barrier model (ToB Ballistic).

distribution function was computed by the QC-BTE until convergence.

C. Device Structure and Poisson's Equation

The targeted device structure is shown in Fig. 1. The transport orientations and sidewalls of the targeted NWs are [001]/(010)/(100), [110]/(1$\bar{1}$0)/(001), [111]/(1$\bar{1}$0)/($\bar{1}\bar{1}$2), and [112]/(1$\bar{1}$0)/($\bar{1}\bar{1}$1). The cross section is a square with 2-nm (Ge) or 1.9-nm (Si) width and height. The 0 V of gate voltage V_G was defined so that the ballistic drain current by a top of the barrier (ToB) ballistic model [7] is 2×10^{-10} A. V_G of 0 V and −0.6V are defined as OFF- and ON-state, respectively. The drain voltage was fixed at −0.6 V. The electrostatic potential inside the NW cross section was fixed as the ballistic result with corresponding bias condition.

To calculate the potential profile along the transport direction, a one-dimensional Poisson equation using the capacitance C_{1D} between the gate and the NW channel was adopted. Defining the electrostatic potential relative to the ballistic result as $\phi(x)$, the carrier line density in the ballistic result as $n_{1D,0}$, the one-dimensional Poisson equation in the channel (cross-sectional area S, dielectric constant ϵ) is given as

$$\phi(x) = \frac{1}{C_{1D}}\left[e\left(n_{1D}(x) - n_{1D,0}\right) + \epsilon S\frac{d^2}{dx^2}\phi(x)\right], \qquad (4)$$

where the hole line density at x is given as $n_{1D}(x)$.

III. Results and Discussion

In Fig. 2, the computed electrostatic and quantum-corrected potentials in the Ge [110] NW pMOSFET at the OFF-state (V_G = 0 V) are compared. The reduction of potential barrier due to quantum correction expresses the impact of tunnel effect.

In the following, the drain currents of Ge [110] and Si [110] NW pMOSFETs are compared and discussed based on the current flux distribution. Then, the orientation dependence and gate length dependence of the performance of Ge NW pMOSFETs are discussed.

A. Drain Current-Gate Voltage Characteristics

In Fig. 3 (a), the calculated drain current-gate voltage characteristics of the Ge [110] and Si [110] NW pMOSFETs are presented. Comparing the results by the QC-BTE with ballistic results (ToB Ballistic), the reduction of ON-current and the increase of OFF-leakage are confirmed. These originate from the impact of scattering and tunneling, respectively. The tunnel leakage is larger in the Ge NW than in the Si NW because of the lighter effective mass of Ge.

To compare the ON-currents of the Ge and Si NW pMOSFETs in a fair way, the V_G values were shifted so that the drain current is 2×10^{-10} A at V_G = 0 V (Fig. 3 (b)). Since the tunnel leakage is larger in the Ge NW, the amount of required V_G shift to suppress tunnel leakage is also larger in the Ge NW. Larger V_G shift means the shift of drain current-gate voltage curve to the left, leading to larger reduction of ON-current. However, the ON-current is still larger in the Ge one (and the difference is larger than the cross-sectional area difference of about 10%). This confirms that the Ge NW has a better quasi-ballistic hole transport capability though the superiority to Si is not so large.

B. Analysis Based on Forward and Backward Currents

To analyze the mechanism of large current of the Ge NW pMOSFET, the forward, backward, and total current distributions at the ON-state after V_G shift in the Ge and Si NW pMOSFETs are compared in Fig. 4. The transmission coefficient T at the ToB is defined as the total current divided by the forward current at the ToB: $T(\mathrm{ToB}) = I_{\mathrm{tot}}/I_{\mathrm{f}}(\mathrm{ToB})$. Despite the higher hole mobility in Ge NWs than in Si NWs, the T(ToB) values of Ge and Si devices were similar. This is attributed to the slower energy relaxation in Ge NWs than in Si NWs [8], resulting in longer distance where holes keep sufficient kinetic energy to return to the source and thus backscattering contributes to current reduction [9]. This means that, in the quasi-ballistic regime, the positive impact of higher mobility (smaller impact of backscattering) of Ge is cancelled by the slower energy relaxation, and therefore the larger current in the Ge NW pMOSFET than in the Si counterpart is

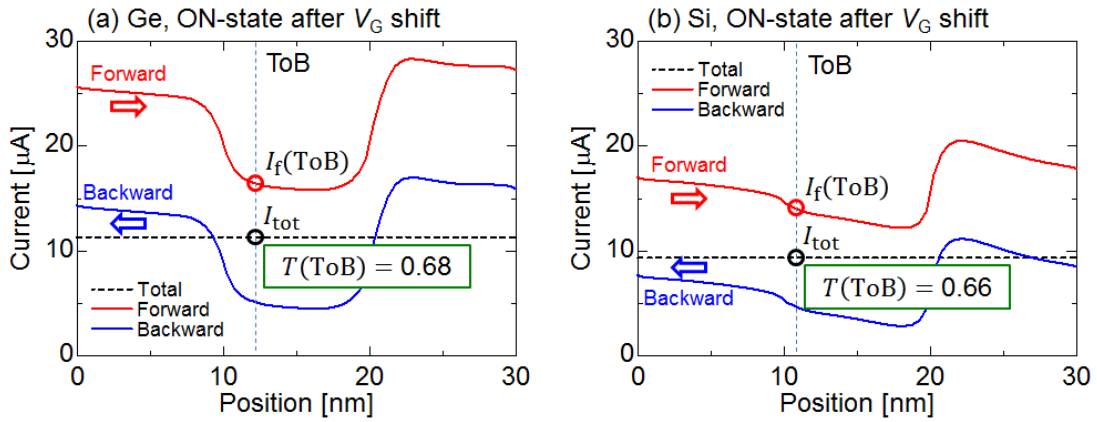

Fig. 4: Current distributions in (a) Ge and (b) Si NW pMOSFETs at the ON-state after V_G shift computed by the QC-BTE. The red and blue lines show the forward and backward currents, respectively. The black dashed lines show the total current, which is the difference between the red and blue lines and is uniform along the device. The transmission coefficient extracted at the top of the potential barrier $T(\mathrm{ToB}) = I_{tot}/I_f(\mathrm{ToB})$ was similar between Ge and Si.

attributed to the larger injection current I_f(ToB), reflecting the larger ballistic current of Ge.

C. *Orientation Dependence of Drain Current of Ge NW pMOSFETs*

Fig. 5 shows the comparison of drain current-gate voltage curves of square cross-sectional Ge NW pMOSFETs with various orientations (a) before and (b) after the V_G shift. These results indicate that, despite the largest OFF-current (before V_G shift) of the [110] NW and the resulting largest amount of V_G shift, the [110] NW exhibits the largest ON-current even after V_G shift.

When longer L_G is adopted and the tunnel leakage current is reduced, V_G shift is reduced. Thus, the drain current-"shifted V_G" curves of the NW orientations suffering from a large tunnel leakage may be improved. Since this improvement by longer L_G is expected to be largest in the [110] NW, which showed the largest tunnel leakage before the V_G shift, the result of largest ON-current in the [110] NW will be maintained even when longer L_G is considered. Actually, the ON-currents of the [001], [111] and [112] NWs before V_G shift are smaller than the ON-current of the [110] NW after V_G shift.

D. *Gate Length Dependence of Drain Current of Ge NW pMOSFETs*

Though the above result showed that the Ge [110] NW has the highest on-current both before and after V_G shift among the considered Ge NWs, its largest OFF-current before V_G shift (or its largest V_G shift) suggests that extending L_G may lead to improved drain current-gate voltage characteristics after V_G shift. Thus, the drain current-gate voltage curves of Ge [110] NW pMOSFETs with various L_G are compared in Fig. 6, and the obtained potential profiles at the OFF- and ON-states (V_G = 0 V and −0.6 V before V_G shift, respectively) are also shown in Fig. 7.

The ON-current before V_G shift decreases with increasing L_G (Fig. 6(a)) as expected, accompanying drastic improvement of OFF-leakage from L_G = 10 nm to 15 nm. This causes the highest on-current at L_G = 15 nm after V_G shift as shown in Fig. 6(b). The L_G of 20 nm does not give additional improvement because additional OFF-leakage reduction is small and long L_G degrades ON-current due to scattering. Therefore, it is concluded that the [110]-oriented Ge nanowire pMOSFETs with 15–20-nm L_G are suitable to achieve a good balance of OFF-leakage and ON-current among the devices considered in this study.

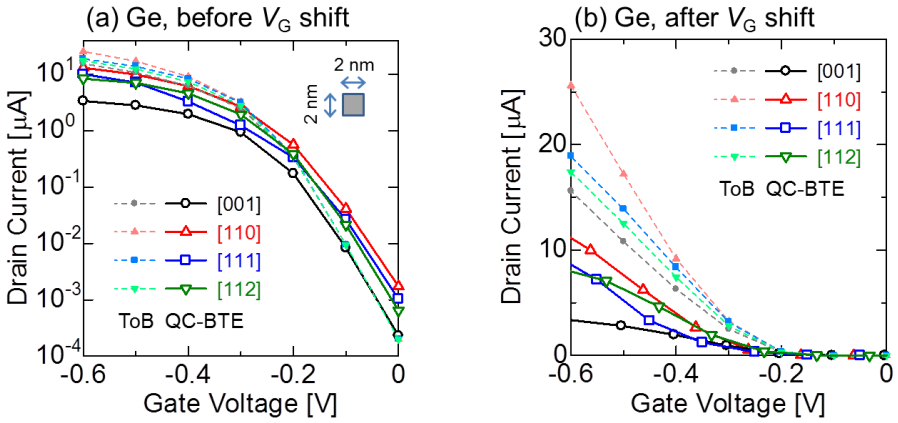

Fig. 5: Calculated gate voltage dependence of drain current in the Ge NW pMOSFETs with various orientations (a) before and (b) after V_G shift. The results calculated by the quantum-corrected Boltzmann transport equation (QC-BTE) are shown by solid lines and open symbols, while the ballistic currents by the top of the barrier model (ToB) are also shown by dashed lines and closed symbols for comparison.

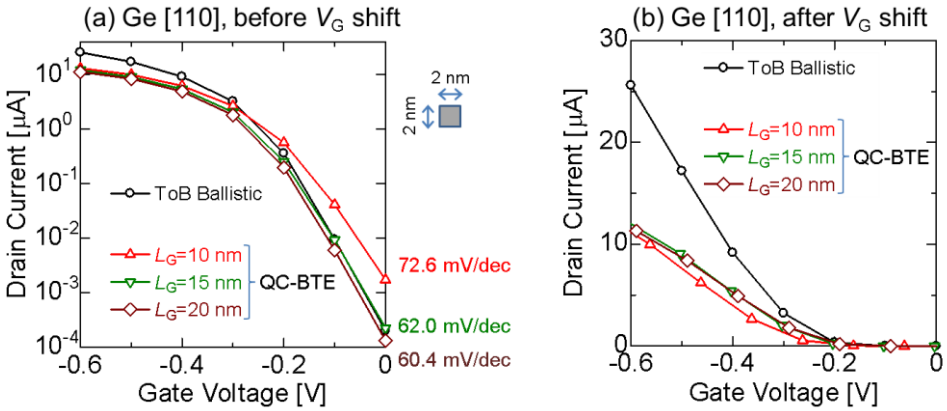

Fig. 6: Calculated gate voltage dependence of drain current in the Ge [110] NW pMOSFETs with various gate lengths L_G (a) before and (b) after V_G shift. The results calculated by the quantum-corrected Boltzmann transport equation (QC-BTE) are shown by red triangles (L_G = 10 nm), green triangles (L_G = 15 nm), and brown diamonds (L_G = 20 nm). The ballistic current by the top of the barrier model (ToB Ballistic) is shown by black circles. The drain voltage was fixed at −0.6 V.

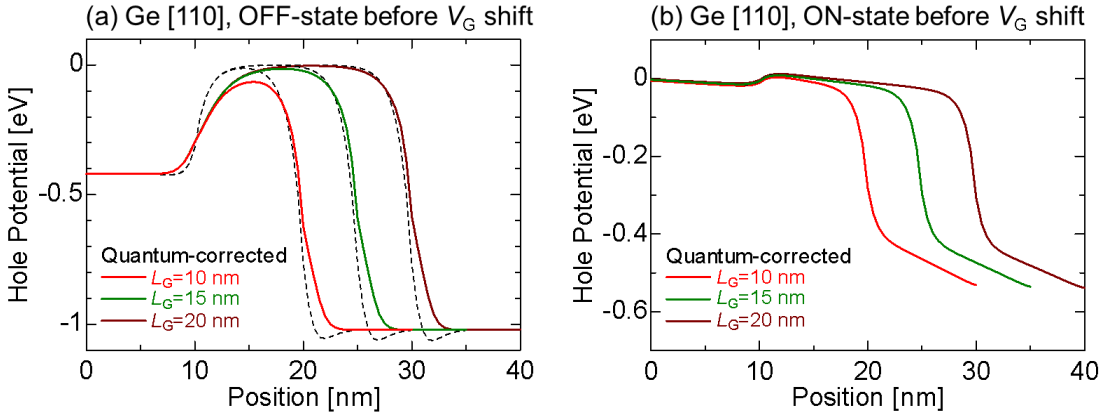

Fig. 7: Steady-state potentials in the Ge [110] NW pMOSFET ((a) OFF- and (b) ON-states) with various gate lengths L_G in the calculation by the quantum-corrected Boltzmann transport equation. The color solid lines and black dashed lines (in (a)) show the quantum-corrected and classical hole potentials, respectively. At the ON-state, the quantum-corrected and classical hole potentials are almost the same, thus the classical potential is not indicated. The drain voltage was −0.6 V. The energy is referenced from the channel potential by the top of the barrier model in the ballistic case.

IV. Conclusion

In this study, the quasi-ballistic drain currents in Ge and Si NW pMOSFETs were computed. Here, a newly proposed quantum-correction potential was included in the Boltzmann transport equation. Though the ON-current of the Ge [110] NW pMOSFET outperformed the Si counterpart, the transmission coefficients extracted at the top of the barrier were similar between Ge and Si, which originates from the slower energy relaxation in Ge and a resulting longer length where holes keep sufficient kinetic energy to be backscattered to the source.

When the ON-currents of Ge NW MOSFETs with various transport orientations are compared with a common OFF-current at a gate length of 10 nm, the Ge [110] NW achieved the highest ON-current among the square cross-sectional NWs with about 2-nm width and 2-nm height. On the other hand, extending the gate length to 15 nm caused remarkable reduction of the tunnel leakage in the [110] Ge NW pMOSFET, and led to the highest ON-current among the devices considered in this study.

References

[1] H. Wu, W. Wu, M. Si, and P. D. Ye, "Demonstration of Ge Nanowire CMOS Devices and Circuits for Ultimate Scaling" IEEE Trans. Electron Devices, vol 63, pp. 3049-3057, August 2016.

[2] H. Tsuchiya, B. Fischer, and K. Hess, "A full-band Monte Carlo model for silicon nanoscale devices with a quantum mechanical correction of the potential," in IEDM Tech. Dig., pp. 283-286, 2000.

[3] E. Wigner, "On the Quantum Correction For Thermodynamic Equilibrium," Phys. Rev., vol. 82, pp. 749-759, June 1932.

[4] Y. M. Niquet, D. Rideau, C. Tavernier, H. Jaouen, and X. Blase, "Onsite matrix elements of the tight-binding Hamiltonian of a strained crystal: Application to silicon, germanium, and their alloys," Phys. Rev. B, vol. 79, 245201, June 2009.

[5] Z. Sui and I. P. Herman, "Effect of strain on phonons in Si, Ge, and Si/Ge heterostructures," Phys. Rev. B, vol. 48, pp. 17938-17953, December 1993.

[6] W. Zhang, C. Delerue, Y. M. Niquet, G. Allan, and E. Wang, "Atomistic modeling of electron-phonon coupling and transport properties in n-type [110] silicon nanowires," Phys. Rev. B, vol. 82, 115319, September 2010.

[7] A. Rahman, J. Guo, S. Datta, and M. S. Lundstrom, "Theory of Ballistic Nanotransistors," IEEE Trans. Electron Devices, vol. 50, pp. 1853-1864, September 2003.

[8] H. Tanaka, J. Suda, and T. Kimoto, "Analysis of High-Field Hole Transport in Germanium and Silicon Nanowires Based on Boltzmann's Transport Equation," IEEE Trans. Nanotechnol., vol. 16, pp. 118-125, January 2017.

[9] H. Tanaka, J. Suda, and T. Kimoto, "Theoretical Analysis of Quasi-ballistic Hole Transport in Ge and Si Nanowires Focusing on Energy Relaxation Process," in Silicon Nanoelectronics Workshop, pp. 35-36, 2017.